REPORT DOCUMENTATION PAGE

Form Approved
OMB No. 0704-0188

1. REPORT DATE *(DD-MM-YYYY)*	**2. REPORT TYPE**	**3. DATES COVERED** *(From - To)*
Dec 2014	Technical Paper	Dec 2014- Jan 2015

4. TITLE AND SUBTITLE

Prediction of Combustion Instability with Detailed Chemical Kinetics

5a. CONTRACT NUMBER
N/A

5b. GRANT NUMBER

5c. PROGRAM ELEMENT NUMBER

6. AUTHOR(S)

Sardeshmukh, S., Anderson, W., Harvazinski, M. and Sankaran, V.

5d. PROJECT NUMBER

5e. TASK NUMBER

5f. WORK UNIT NUMBER
Q12J

7. PERFORMING ORGANIZATION NAME(S) AND ADDRESS(ES)

Air Force Research Laboratory (AFMC)
AFRL/RQR
5 Pollux Drive
Edwards AFB CA 93524-7048

8. PERFORMING ORGANIZATION REPORT NO.

9. SPONSORING / MONITORING AGENCY NAME(S) AND ADDRESS(ES)
Air Force Research Laboratory (AFMC)
AFRL/RQR
5 Pollux Drive
Edwards AFB CA 93524-7048

10. SPONSOR/MONITOR'S ACRONYM(S)

11. SPONSOR/MONITOR'S REPORT NUMBER(S)
AFRL-RQ-ED-TP-2014-383

12. DISTRIBUTION / AVAILABILITY STATEMENT
Distribution A: Approved for Public Release; Distribution Unlimted.

13. SUPPLEMENTARY NOTES
Briefing Charts presented at AIAA SciTech 2015, Kissimmee, FL, 5-9 January 2015.

14. ABSTRACT

Combustion instability in an unstable single element rocket chamber using methane as the fuel is computationally studied. Effects of the kinetics mechanism are examined by comparing the results using a single step global mechanism and a detailed mechanism with 32 species and 177 reactions. Significant differences between the two predictions are identified including the amplitude of the unsteady pressure oscillations, and more importantly, the underlying mechanisms responsible for driving the combustion instabilities.

15. SUBJECT TERMS

16. SECURITY CLASSIFICATION OF:			**17. LIMITATION OF ABSTRACT**	**18. NUMBER OF PAGES**	**19a. NAME OF RESPONSIBLE PERSON**
					Venke Sankaran
a. REPORT	**b. ABSTRACT**	**c. THIS PAGE**	SAR	20	**19b. TELEPHONE NO** *(include area code)*
Unclassified	**Unclassified**	**Unclassified**			661-275-5534

Standard Form 298 (Rev. 8-98)
Prescribed by ANSI Std. 239.18

Prediction of Combustion Instability with Detailed Chemical Kinetics

Swanand V. Sardeshmukh*[1], William E. Anderson†[1], Matthew E. Harvazinski,‡[2] and Venkateswaran Sankaran,§[2]

[1] *Purdue University, W. Lafayette*
[2] *Air Force Research Laboratory (AFRL), Edwards AFB.*

Combustion instability in an unstable single element rocket chamber using methane as the fuel is computationally studied. Effects of the kinetics mechanism are examined by comparing the results using a single step global mechanism and a detailed mechanism with 32 species and 177 reactions. Significant differences between the two predictions are identified including the amplitude of the unsteady pressure oscillations, and more importantly, the underlying mechanisms responsible for driving the combustion instabilities.

I. Introduction

Combustion instability arises when the unsteady combustion heat release couples with the acoustic pressure. Rocket engines are particularly susceptible to combustion instability because they are acoustically compact. Combustion instability mitigation has been a part of nearly every production rocket engine development. The presence of combustion instability in an engine can lead to a rapid catastrophic failure of the engine. The growth of the instability takes place very quickly precluding the use of any active feedback control. Currently, no a-priori model exists which is able to predict instability given a particular configuration and operating condition. The ability to predict the onset of instability is key in reducing the risk in the design and development of new liquid rocket engines.

Recently, combined experimental and computational studies have shown the ability of the simulations to replicate self-excited combustion instabilities in a single element rocket chamber. These studies have utilized the Continuously Variable Resonance Combustor (CVRC), which is a single element model rocket combustor with a shear coaxial fuel injector using gaseous methane as fuel. The oxidizer post length of the CVRC can be changed during the experiment to obtain different levels of self-excited combustion instabilities. The combustor operates at a nominal chamber pressure of 15bar and has a choked flow condition at the inlet of the oxidizer post and at the exit of the combustor, which allow the acoustic modes in the chamber to be well characterized[1].

The CVRC has a high volumetric heat release rate on the order of 100MW/m^3 for methane, compared to typical liquid fueled air breathing engines, which are on the order of 10MW/m^3 [2;3]. The setup consists of a back- step combustion chamber fed by gaseous methane and decomposed hydrogen peroxide. The fuel is injected radially inward on a sleeve which turns the flow in the axial direction with minimal swirl. The oxidizer is decomposed hydrogen peroxide, which is supplied through choked slots that can be translated axially. The short oxidizer post length, 8.89 cm, corresponds to a marginally stable operating condition with peak-to-peak amplitudes of 12%. The long oxidizer post length, 19.05 cm lies at the stability boundary and experiments have indicated both stable and unstable behavior at this condition depending on other

*Post Doctoral Researcher, School of Aeronautics and Astronautics, 701 W. Stadium Ave. W. Lafayette, IN-47907, student member, AIAA.

†Professor, School of Aeronautics and Astronautics, 701 W. Stadium Ave. West Lafayette, IN 47907, Associate Fellow, AIAA.

‡Scientist, Rocket Propulsion Division, Air Force Research Laboratory (AFRL), Edwards AFB, CA 93524, USA, Member, AIAA.

§Senior Scientist, Rocket Propulsion Division, Air Force Research Laboratory (AFRL), Edwards AFB, CA 93524, USA, Member, AIAA.

circumstances such as wall conditions and hysteresis effects. Oxidizer post lengths between these extents are consistently unstable. The 13.97 cm length is the most unstable with peak-to-peak amplitudes of 40% of the mean [1].

The gaseous fuels, choked boundary conditions, and wide range of instability amplitudes make the CVRC experiment amenable to modeling. Significant modeling work has been done by a variety of groups using hybrid RANS/LES models [4–6] and large eddy simulations [7;8]. All prior simulations have used global or 2-step reduced mechanisms. In general two-dimensional simulations were unable to replicate the instability amplitudes seen in the experiment while three-dimensional simulations produced excellent agreement with the experiments for the unstable operating conditions. The stable and marginally stable operating conditions have been more difficult to match. Prior work by Harvazinski et al. has suggested that the instability is caused by the timing of the reflected pressure wave in the oxidizer post and its interaction with a cyclic fuel supply cut off event [6].

It is widely known that global and highly reduced chemical kinetics make large approximations to the actual combustion processes. Global mechanisms are typically tuned to match specific parameters, like ignition delay or laminar flame speed. Because only a few tunable parameters exist in the model it is not possible to match all relevant parameters over a wide range of operating conditions. Combustion in the CVRC is highly complex, regions of premixed, non-premixed, and partially premixed combustion exist at different times and locations of the combustor. Local extinctions and reignition are also present and are key to the instability mechanism. The timing of all of these events is either closely coupled with the chamber acoustics in the unstable case or not coupled in the stable case. These observations suggest that it is necessary to evaluate the effects of including detailed chemical kinetics mechanisms on the prediction of combustion instabilities. This is the objective of the present article. Specifically, we compare the simulations with detailed kinetics with those done with simplified global kinetics to ascertain the differences in the physics of coupling between the combustion and acoustic cycle. All three post-length cases are studied and attention is paid to discerning the specific modes of coupling that lead to the incidence of combustion instability. The mechanisms used for methane oxidation are the GRI 1.2 set that comprises of 32 chemical species and 177 reactions. All the computations performed here use an axisymmetric assumption in order to accommodate the detailed chemical mechanisms efficiently. The computations utilize detached eddy simulations to capture the turbulence in the flame region with laminar combustion closure, consistent with our previous studies using global chemical kinetics.

The present study looks at the effect of chemical kinetics on combustion instability modeling. Three oxidizer post lengths, corresponding to marginally stable, unstable, and stable conditions, are simulated and analyzed. Specifically we compare simulations performed with a single step global reaction and the GRI-1.2 kinetics mechanism which contains 177 reactions. The paper is organized as follows, Section II presents details on the modeling approach including details of the selection of the chemical kinetics mechanism. Section III presents the results of the three simulations. Finally Section IV lists the summary and conclusions.

II. Model

A. Gas Phase Reaction Kinetics

Modeling of the CVRC experiment using CFD has been previously attempted by several researchers [5;7–9]. All of these simulations are similar in that they used simplified reaction mechanisms. Before proceeding with the simulations, detailed analysis of four methane combustion mechanisms is presented. The simplest mechanism is a single global reaction where the fuel and oxidizer react to form water and carbon dioxide. The production of carbon monoxide is a known intermediate step in hydrocarbon oxidation and is included in the two-step reduced mechanism. In both the mechanims, the rate expressions were calibrated to measured laminar flame speeds [10]. GRI-1.2 is a more complete set of hydrocarbon reactions consisting of 177 reactions involving 32 species and was optimized for natural gas combustion at the Gas Research Institute (GRI) [11]. A further refinement of the GRI-1.2 mechanism resulted in GRI-3.0, which includes nitrogen chemistry and higher number of species and reactions. In the CVRC experiment, decomposed hydrogen peroxide is the oxidizer and no nitrogen is present so GRI-3.0 is included for comparison only. All the models discussed here are readily available in literature. The models are summarized in Table 1.

In the CVRC fuel at room temperature is injected upstream of the back step, along the periphery of the hot oxidizer flow as shown in Figure 1. Mixing in this region has been identified as a crucial step of the cyclic heat release process. Furthermore, hot products of combustion, trapped in the recirculation near the

Table 1: Details of the chemical kinetics mechanisms.

	Global-1	Global-2	GRI-1.2	GRI-3.0
Species	CH_4, O_2, CO_2 and H_2O	Global-1 species + CO	33	53
Reactions	1	2	177	325

back-step interact with the cold shear layer as shown in the schematic Figure 1. The state of the mixture therefore varies significantly and the ensuing heat release varies accordingly. To assess the chemical kinetics mechanism three parameters which correspond to the above behavior are investigated. The parameters are the ignition delay, heat release rate, and maximum temperature.

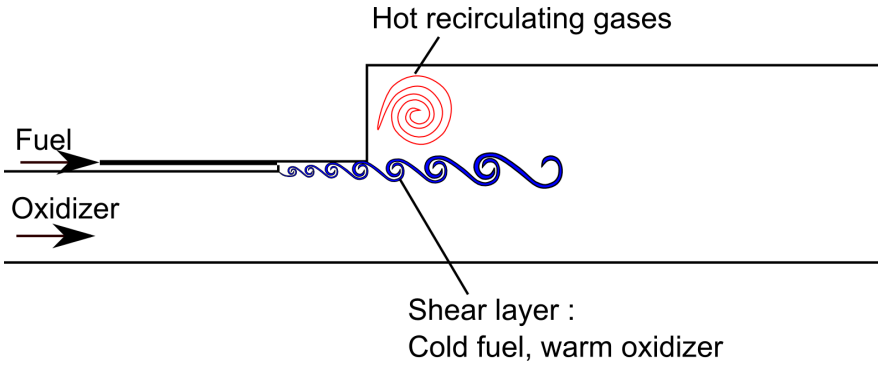

Figure 1: Schematic of flow dynamics in the CVRC Experiment. Fuel-oxidizer mixing in the region shown affects the heat release.

Ignition Delay

Figure 2 shows the ignition delay predictions of the four mechanisms considered as a function of the initial temperature of the mixture and the composition, at a constant pressure of 1.4 MPa. The temperature range applicable to the CVRC is between 1000 K and 1400 K. The lower limit represents 7% by mass of the fuel mixed with the oxidizer. The upper limit is 30% by mass of the combustion gases at 2400 K mixed with the oxidizer and fuel mixture. This range of initial temperatures shows that the ignition delay values predicted by both the global mechanims are an order of magnitude lower in the range of interest. A similar observation has been reported in the literature[12] for a different oxidizer and operating conditions. The global two step mechanism also shows unrealistic ignition delay trend for the rich mixture. Both the detailed mechanisms show ignition delay values of the same order and are closer for near stoichiometric mixtures and at high temperatures.

Temperature

The global mechanisms predict a higher temperature rises from combustion because many intermediate and trace species are neglected. Figure 3 shows the variation in the maximum temperature prediction by the four mechanisms. In the plots the maximum temperature is normalized by the initial temperature. It is clear that the peak temperatures predicted by the global mechanisms exceed those of the detailed kinetics by a factor of 1.3 to 1.5. This affects not only the speed of sound in the mixture but also the interaction between the burnt and unburnt mixtures. The combination of the shorter ignition delay and higher post-flame temperature can initiate combustion earlier in the mixing region which will delay the further mixing of fuel and oxidizer. In two-dimensional simulations the effect would be magnified because of the axisymmetry assumption and

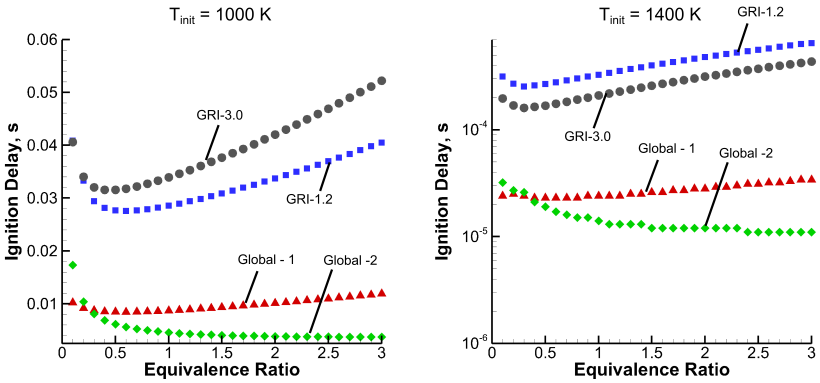

Figure 2: Variation of ignition delay predictions by the four chemical kinetics mechanisms.

may entirely prevent the further mixing of fuel and oxidizer. As a result, this would lead to a stretched heat release zone.

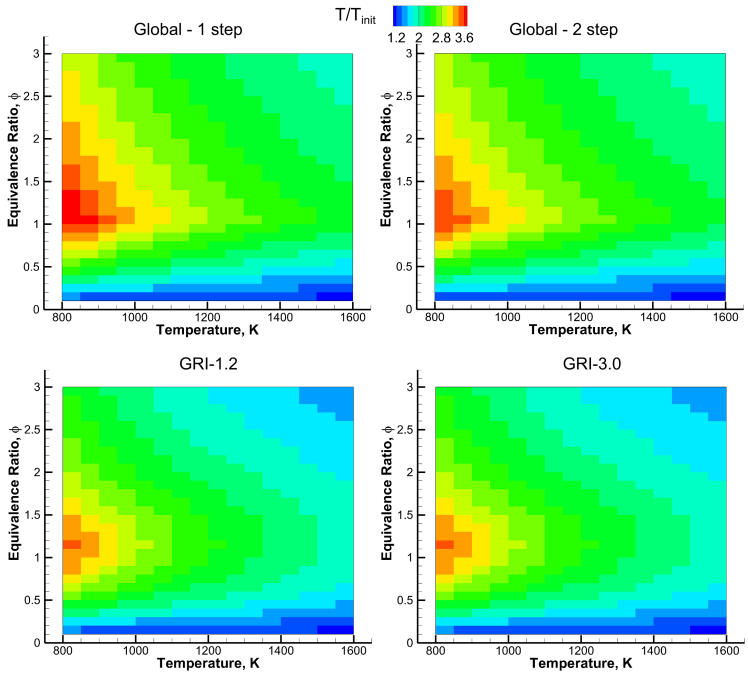

Figure 3: Variation of normalized maximum temperature predictions by the four chemical kinetics mechanisms.

Heat Release Rate

Combustion instability prediction is closely related to the heat release rate prediction and its coupling with the acoustic modes. Figure 4 shows the comparison of the maximum heat release rates for the global-1 and GRI-1.2 mechanisms under consideration. Predictions of the GRI-3.0 and global-2 are close to those shown for GRI-1.2 and global-1 mechanisms respectively. The heat release rate predictions of the global mechanisms exceed those of the detailed kinetics by an order of magnitude and can significantly overpredict the heat release rate, which influences acoustic fluctuations. It is likely that these differences along with those mentioned earlier can materially affect the nature of the combustion stability mechanisms.

Amongst the above results, it is notable that the temperature prediction of the detailed mechanisms is nearly identical. The ignition delay predictions of the two detailed mechanisms are close and the heat release of the GRI-3.0 mechanism, although not shown, resembles the predictions of the GRI-1.2 mechanism. These similarities can be attributed to the fact that the GRI-3.0 mechanism has evolved from the GRI-1.2 mechanism. The GRI-1.2 mechanism is therefore expected to give similar results as the GRI-3.0 mechanism. The remaining results in the paper therefore consider only the GRI 1.2 mechanism and make comparisons with the global-1 mechanism that was used in previous studies.

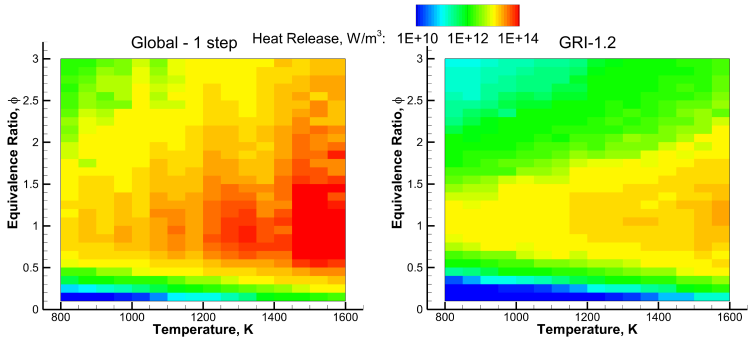

Figure 4: Variation of maximum heat release rate predictions by the two chemical kinetics mechanisms.

Consistent with the previous work, the CFD code GEMS (General Equation and Mesh Solver) is employed in the present work for the computational investigation. GEMS solves the implicitly discretized fully-coupled conservation equations. Dual time stepping is used to eliminate approximate factorization errors. The algorithm is second order accurate in both space and time. Large scale turbulent motions are captured in GEMS with LES (Large Eddy Simulation) while the small scales are modeled using Wilcox's $k-\omega$ model[13], which becomes dominant in the near wall region. Additional details of the code and capabilities can be found in 14, 15, 16, 17, 18.

III. Simulation Results and Discussion

Three cases encompassing the variations of the oxidizer post length are chosen for the study. The three oxidizer post lengths are - 8.89 cm, 13.97 cm and 19.05 cm, which correspond to the marginally stable, unstable and stable operating conditions. The overall operating condition is fuel lean, with fuel to oxidizer ratio by mass of 0.85 or equivalence ratio of 0.72. A choked nozzle at the downstream boundary of the combustor creates a pressure anti-node. Likewise, the inlet oxidizer flow is choked through a series of slots, which are approximated by a constant mass flux computation in the present calculations. Adiabatic, non-slip walls are assumed for the fuel and oxidizer post as well as for the chamber walls.

The experimental measurements include pressure probes located along the length of the combustion chamber. For comparison with the computations, the pressure probe located at the anti-node near the downstream end of the combustor is chosen for its reduced susceptibility to local variations and ability to capture limit cycle behavior. An overall comparison of experimental and computed pressure trace for the three oxidizer post lengths is shown in Figure 5. Both the global reaction and the detailed chemical kinetics show limit cycle behavior in all the cases shown. The pressure signals from the global-1 simulations show more noise compared to the GRI-1.2 simulations. Importantly, in the case of the two shorter oxidizer post lengths, the signal correspondence between experiment and simulations is improved along with the peak-to-peak amplitude of the pressure. Particularly, for the highest amplitude instability case at a length of 13.97 cm, the detailed kinetics result agrees remarkably well with the experimental peak-to-peak magnitude, while the global-1 result appears to under-predict this by more than 50%. Predictions for the longest oxidizer post length exceed the observed magnitude of the instability. It should however be recognized that there is some modulation in the experimental pressure. The peak-to-peak pressure variation shows a maximum difference of 200 kPa, which is comparable to the global kinetics predictions.

Frequency content and the power corresponding to the dominant pressure modes is considered next and is shown in Figure 6. In all three cases, the global kinetics result shows that the frequency of the first acoustic

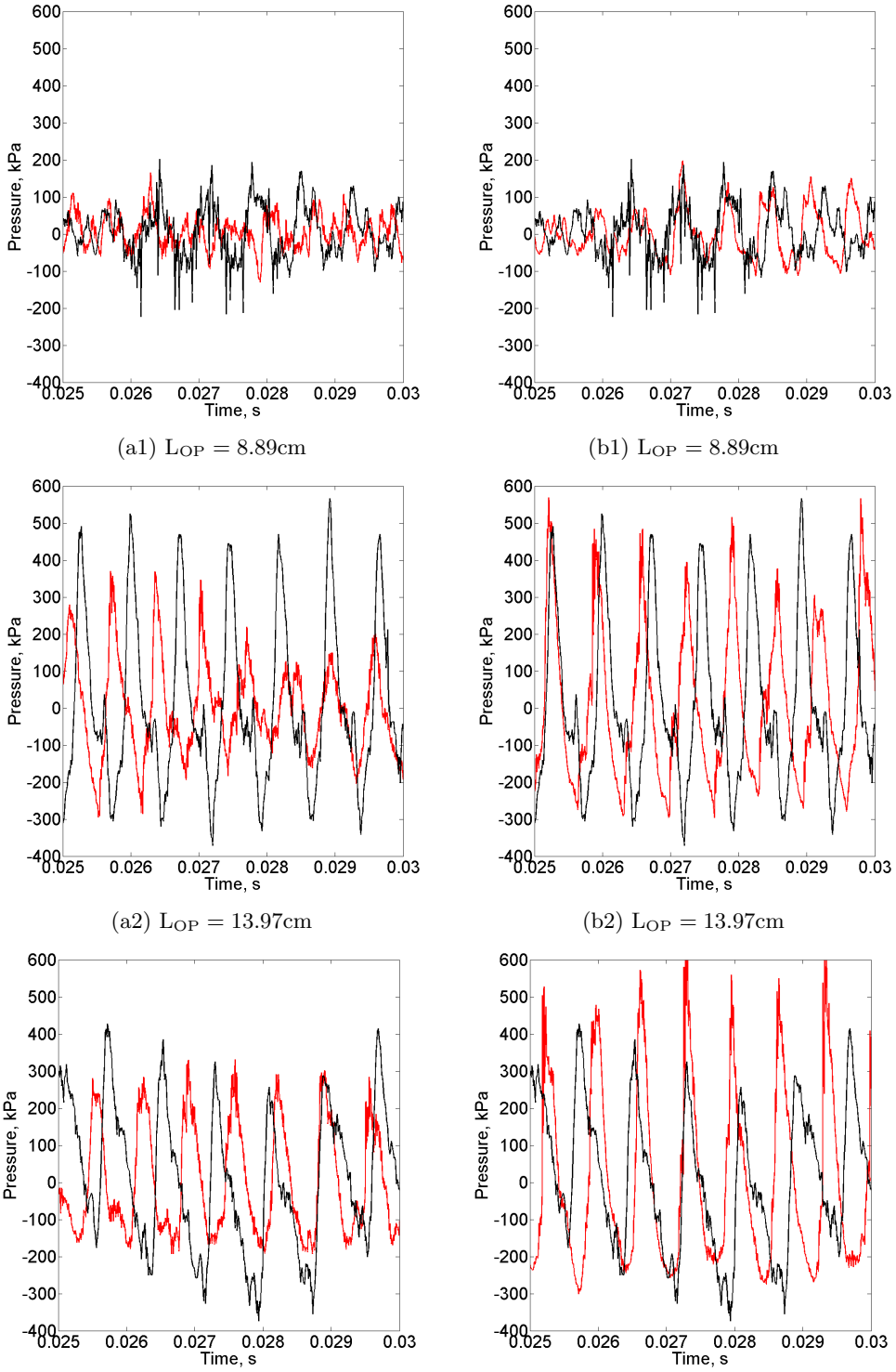

(a1) L_{OP} = 8.89cm

(b1) L_{OP} = 8.89cm

(a2) L_{OP} = 13.97cm

(b2) L_{OP} = 13.97cm

(a3) L_{OP} = 19.05cm

(b3) L_{OP} = 19.05cm

(a) Global single step kinetics

(b) Detailed, GRI-1.2 kinetics

Figure 5: Pressure trace comparison for the three oxidizer post lengths. Pressure probe located at an axial position of 0.3683 m, near the wall.

mode is over-predicted by about 15-20%. In contrast, the detailed kinetics results appear to be improved with the frequency predictions now being about 10% higher than the experiments. This improvement is because the equilibrium temperature of the flame is lower (as is the sound speed) on account of the larger number of chemical species included in the detailed kinetics. The remaining frequency discrepancy is probably due to the use of an adiabatic wall boundary; the inclusion of the wall heat flux would likely further reduce the temperature and the sound speed and, consequently, the acoustic frequency. It is also evident that the amplitude of the modes are also improved by the inclusion of detailed kinetics, especially in the case of the two unstable lengths - i.e., post-lengths of 13.97 cm and 19.05 cm. An exception to this is the second mode of the 13.97 cm, which is predicted to be about the same for both the global and detailed kinetics cases. Still, one might note that the general trend is that the detailed kinetics predictions show sharper resolution of the higher harmonics, even if the amplitudes continue to be somewhat under-predicted.

In addition to these comparisons, the simulations can also aid in developing the understanding of the physics involved in the unstable combustion with the two longer oxidizer post lengths and clarify possible differences in the case of marginally stable shorter oxidizer post length. The following subsections present detailed results from each of the oxidizer post lengths, the unstable operating condition is considered first.

A. Unstable Operating Condition

Experimental chemiluminescence images of the near back-step combustion behavior through two radical species CH^* and OH^* have been obtained for all three oxidizer post-lengths. Both of the species have been used as markers of heat release in various experiments [19;20], but modeling of these radicals has been limited to relatively simple flames [21] and rare in multi-dimensional simulations [22]. A major difficulty in their inclusion as a computed species lies in the absence of their source species in the kinetics mechanisms that are typically used for the simulations. With the detailed kinetics like the GRI-1.2, this no longer is the case and both CH^* and OH^* can be computed as quasi-steady species in a post-processing step with minimal computational cost. The assumption of quasi-steadiness can be expected to be better held for the CH^* than OH^* because of its lower concentrations [19].

Phase averaged pressure cycle at the head end of the combustor is shown in Figure 7a. Corresponding visual comparison for selected of the phase averaged CH^* inverse-Abel transformed experimental images with phase averaged axisymmetric computations is shown in Figure 7b. At the start of the cycle, during pressure rise, high intensity is seen near the wall of the combustor. At or near the peak pressure (cycle point 3), the high intensity region displays a shift away from the wall. Pressure in the head end decreases from cycle points 7 to 15, while the luminosity of the CH^* radicals indicates reduced number density. Towards the end of the cycle, points 18 to 20 show increasing intensity, marking the beginning of the next cycle. The same structural sequence can be seen in the computed CH^* radical. Simulation results suggest that the sequence of events starts with a partially mixed fuel-oxidizer jet hitting the combustor wall and rolling up to form two vortices. The upstream vortex interacts with the recirculation zone near the back step of the combustor and the fuel-oxidizer mixture in the shear layer to form a high concentration CH^* region. A more detailed cycle analysis with the help of computational result of the GRI-1.2 mechanism is presented next.

To understand the coupling between the unsteady heat release and the acoustics of the combustor, captured by GRI-1.2 mechanism, a representative cycle is selected for analysis. The pressure at the head end for the cycle is shown in Figure 8, from the GRI-1.2 simulation. Five points are marked on the cycle and correspond to the detailed contour plots shown in Figure 9. Figure 9 shows the pressure, heat release, fuel mass fraction and axial velocity. At the beginning of the cycle high pressure is generated near the back step of the combustor. As this pressure wave travels upstream in the oxidizer post, the velocity decreases. Consumption of the fuel present within the combustor is nearly complete and the heat release is decreasing as a consequence. The hot combustion products drive the axial velocity in the downstream section of the combustor, leading to enhanced mixing. High temperature in this region accelerates the consumption of the residual fuel.

Moving to the second point of analysis the pressure at the head end decreases. The rapid fuel consumption seen from time 1 along with the upstream traveling high pressure wave in the oxidizer post cuts off the fuel supply to the reacting region. The adverse pressure gradient at the front of this pressure wave acts to decrease the shear within the oxidizer post. In the combustor, the high velocity products move downstream, reducing the shear near the back step. The combination of reduced mixing and fuel cut-off allows fuel in the combustor to remain unreacted, visible at time 3. At this point in the cycle, the reflected pressure wave from the oxidizer post arrives near the lip of the fuel sleeve, where increased shear due to high velocity enhances

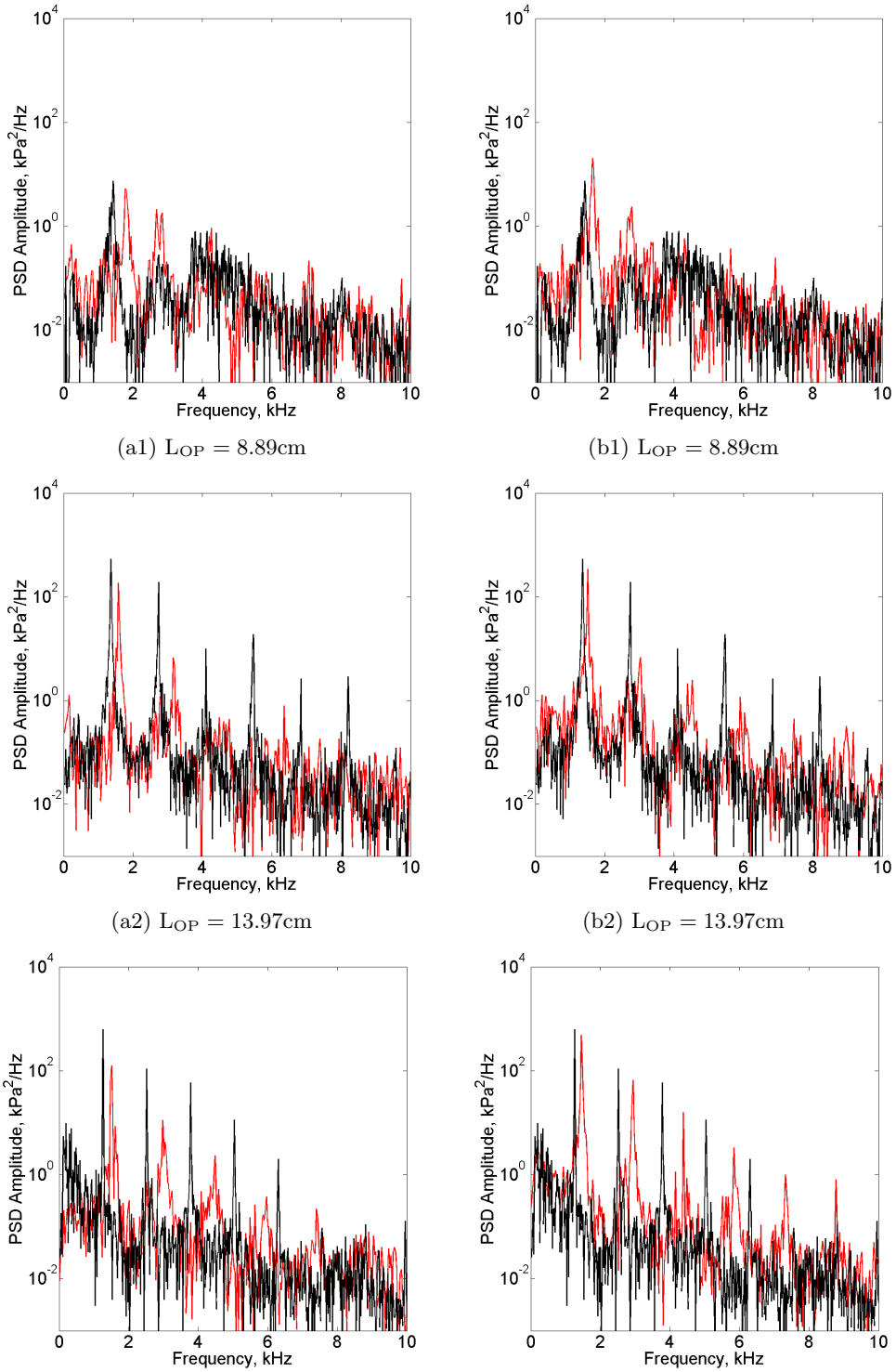

(a1) $L_{OP} = 8.89$cm (b1) $L_{OP} = 8.89$cm

(a2) $L_{OP} = 13.97$cm (b2) $L_{OP} = 13.97$cm

(a3) $L_{OP} = 19.05$cm (b3) $L_{OP} = 19.05$cm

(a) Global single step kinetics (b) Detailed, GRI-1.2 kinetics

Figure 6: Comparison of the spectral power for the three oxidizer post lengths corresponding to the pressure trace shown in Figure 5.

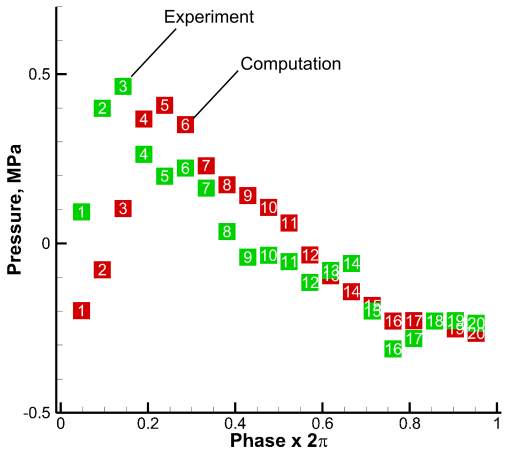

(a) Comparison of phase averaged pressure cycle at the head end

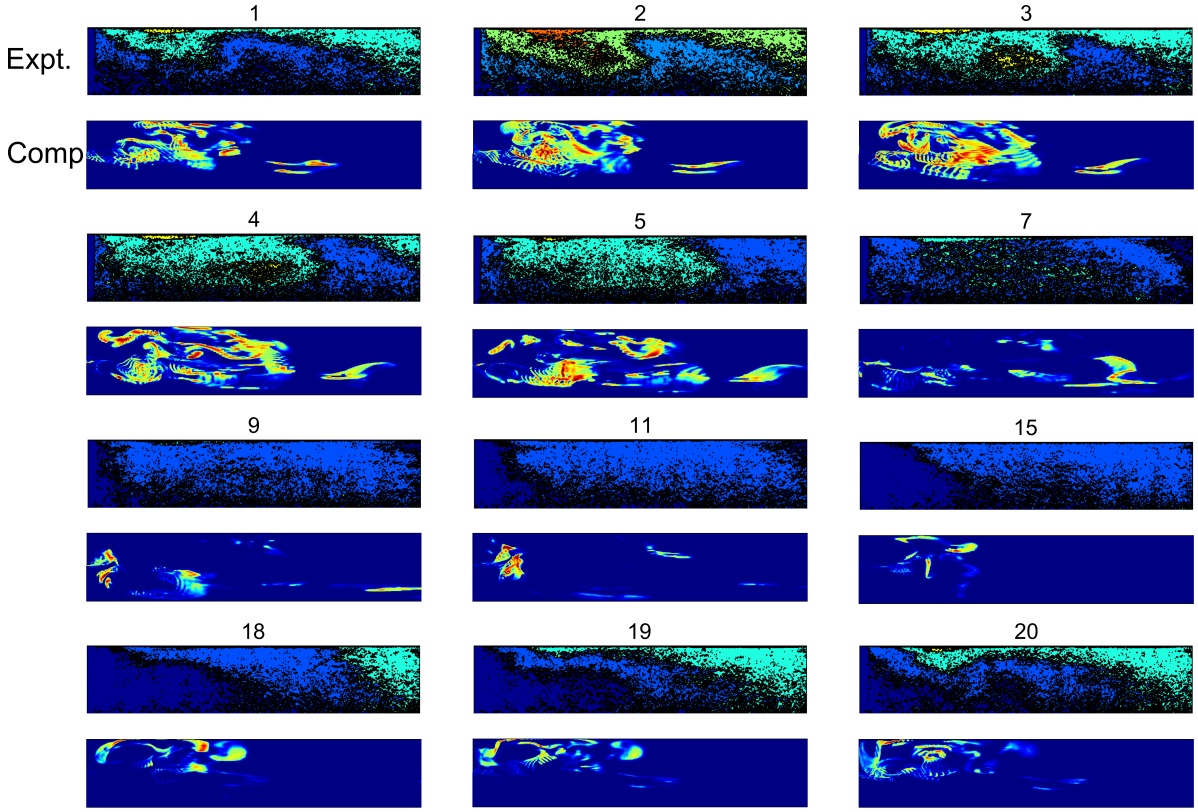

(b) Comparison of selected inverse Abel transformed CH^* radical images from the experiments and the computations

Figure 7: Comparison of the phase averaged chemiluminescent species during the cycle

mixing. Axial velocity near the back step remains low, in turn affecting the mixing and thus maintaining low rate of fuel consumption. This is evident from the low heat release rate.

At time 4 of the cycle, the reflected pressure wave from the oxidizer post passes into the combustor, increasing the velocity at the back step. Increased mixing of the fuel, oxidizer and the recirculating hot products of combustion can be deduced from the fuel mass fraction contours. Similarly, mixing also occurs

near the combustor wall where the jet of fuel-oxidizer mixture rolls up to form the two vortices shown. As the pressure wave reflected at the downstream boundary arrives, the upstream of the two vortices moves towards back step, transporting the unburnt mixture in the vicinity of the recirculating hot products. This also causes the hot gas near the back step to move radially inwards, close to the shear layer.

Figure 10a shows variation in local equivalence ratio between the limits of $\phi = 0.35$ and $\phi = 3.5$ at this instance. The shear layer is clearly seen from the scatter-plot, wherein the data points are sized with local equivalence ratio and colored by temperature of the mixture. Top edge of the shear layer displays high temperatures on account of its interaction with the recirculating hot products. The ignition delay in this region therefore is expected to be orders of magnitude smaller in comparison to the bottom edge of the shear layer. The bottom edge of the shear layer, with temperature close to that of the oxidizer, continues to get entrained in the upstream vortex. Recalling the variation of the ignition delay in the rich branch of the mixture (Figure 2), burning in the shear layer will largely be controlled by mixing.

As a qualitative measure of unmixedness in this region, the standard deviation of the equivalence ratio is shown in Figure 10b as a time series along with the pressure. A clear trend is visible, a drop in the standard deviation or increased uniformity of the mixture leads to a rapid pressure rise. Accumulation of the fuel can also be deduced from this plot. Increasing unmixedness at a given temperature implies greater overall ignition delay. Increased induction period permits better mixing and partial conversion of the fuel. It must be kept in mind that the significant difference between global kinetics and detailed kinetics is the partial conversion, which can allow coherent heat release from mixtures at different states.

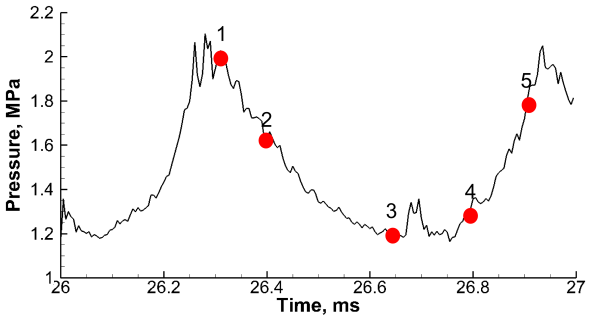

Figure 8: Pressure cycle chosen for detailed analysis of the oxidizer post length 13.97cm

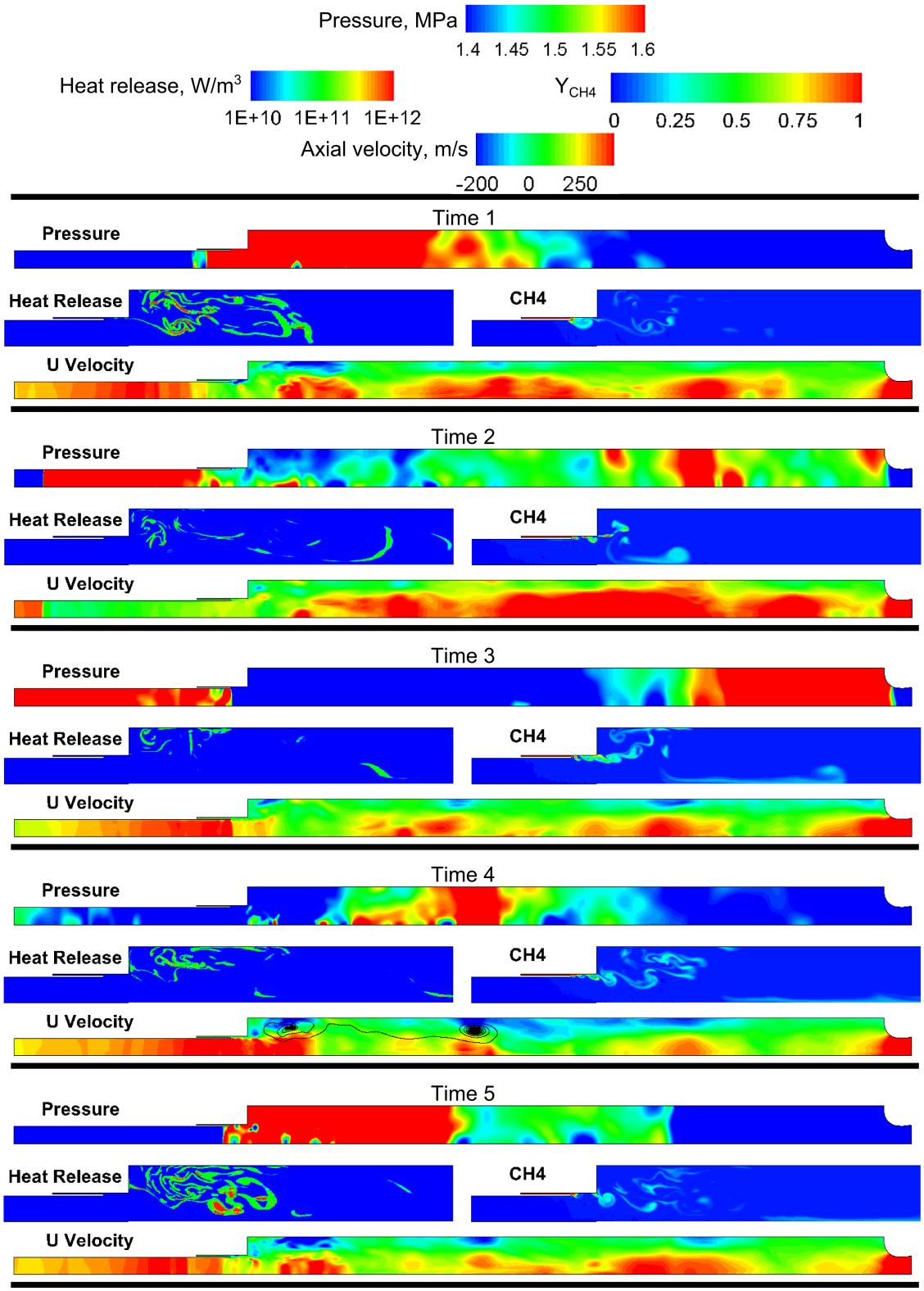

Figure 9: Limit cycle analysis for $L_{OP} = 13.97$cm

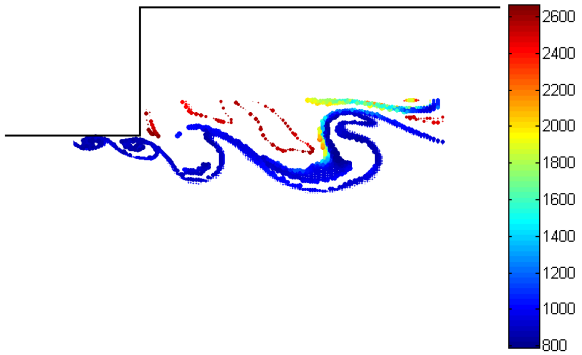

(a) Shear layer, shown by scatter of data. The markers are sized with the equivalence ratio and colored by the temperature of the mixture.

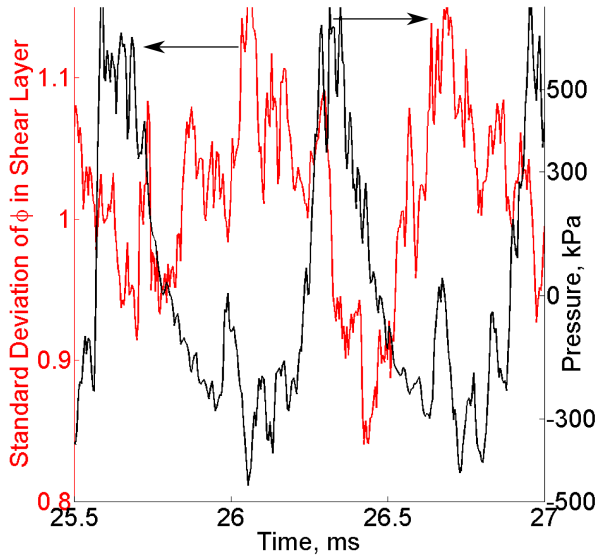

(b) Unmixedness in the shear layer indicated by standard deviation of the equivalence ratio.

Figure 10: Shear layer dynamics for the oxidizer post length of 13.97cm, marked by equivalence ratio and mixture temperature in relation to the local pressure

B. Marginally Stable Operating Condition

The shorter oxidizer post length (8.89 cm) is a marginally stable operating point for the CVRC experiment. It is therefore of interest to contrast the findings of the unstable and marginally stable simulations with the GRI-1.2 kinetics. A cycle representative of the limit cycle behavior is shown in Figure 11. Corresponding details of the flow-field are shown in Figure 12. Pressure fluctuations in this case remain moderate, which can be seen at the start of the cycle. The lower pressure amplitude in this case can be attributed to the spread of the fuel consumption along the axial direction.

At time 2, the reflected pressure wave from the oxidizer post arrives at the dump plane of the combustor, which is earlier than the previous case. The pressure wave in the combustor has not yet reached the downstream boundary. The increased velocity as the pressure wave exits the oxidizer post induces better mixing in the shear layer. Compared to time 1, the heat release does not diminish significantly. It is noteworthy that the uninterrupted consumption of fuel signifies hot products moving at higher velocities through the combustor, therefore aiding the mixing and distributing the heat release in the combustor. At time 3 of the cycle, the fuel consumption near the back step is slightly reduced. However, a favorable pressure gradient during the previous step continues to drive the high velocity near the dump plane. The flowfield at time 4 of the cycle shows increased heat release prior to the arrival of the reflected pressure wave in the combustor. The last snapshot shows heat release occurring throughout the domain.

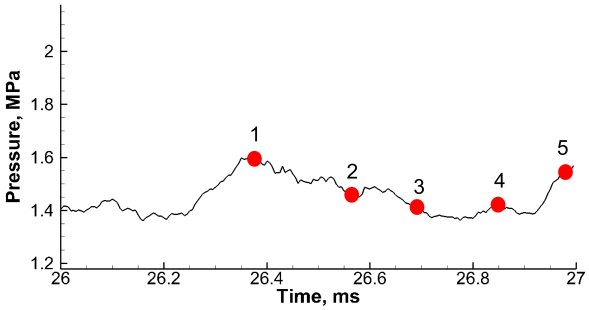

Figure 11: Pressure cycle chosen for detailed analysis of the oxidizer post length 8.89 cm.

Figure 13 shows the standard deviation of equivalence ration within the shear layer in the case of the shorter oxidizer post length. It shows limited variation, suggesting continuous processes. The importance of mixing in the oxidizer post and the shear layer close to the dump plane can be affirmed from this trend.

C. Unstable Operating Condition - Long Length

In the CVRC experiment, both stable and unstable operation can be found for the long oxidizer post length. Both axisymmetric two-dimensional and three-dimensional simulations with global kinetics have predicted unstable operation of the CVRC at the oxidizer post length of 19.05 cm. Simulations with GRI-1.2 also predict an unstable mode of the CVRC at the longer oxidizer post length. This is possibly due to the assumption of adiabatic wall boundary condition in the simulation. The flowfield predicted with detailed kinetics is described below, which gives some insights into the observed trends.

A representative pressure cycle is shown in Figure 14, the flowfield is shown in Figure 15. Although the overall cycle bears resemblance to the one described in Section A, there is a difference in the mechanism of instability for the longer oxidizer post length. At time 1, the initial high pressure wave is generated by the rapid fuel consumption and heat release. The upstream traveling wave causes the fuel to move radially inward, constituting a cross flow in the high speed oxidizer stream. It should be recognized that such an obstruction of the oxidizer flow due to axisymmetric assumption is unrealistic and will not occur in 3-D simulations. In this case, it marks the separation between the fuel consumption and accumulation events.

At time 2 of the cycle, the fuel accumulation and reduced heat release close to the back step of the combustor is visible. At the same time, the pressure at the combustor head end is lower than the downstream end of the upstream traveling pressure wave. This favorable pressure gradient leads to an increase in the axial velocity at the dump plane. This increase in axial velocity drives the roll-up of the shear layer close to the back step, visible at time 3. Relatively less mixed fuel and oxidizer form the two vortices similar to those

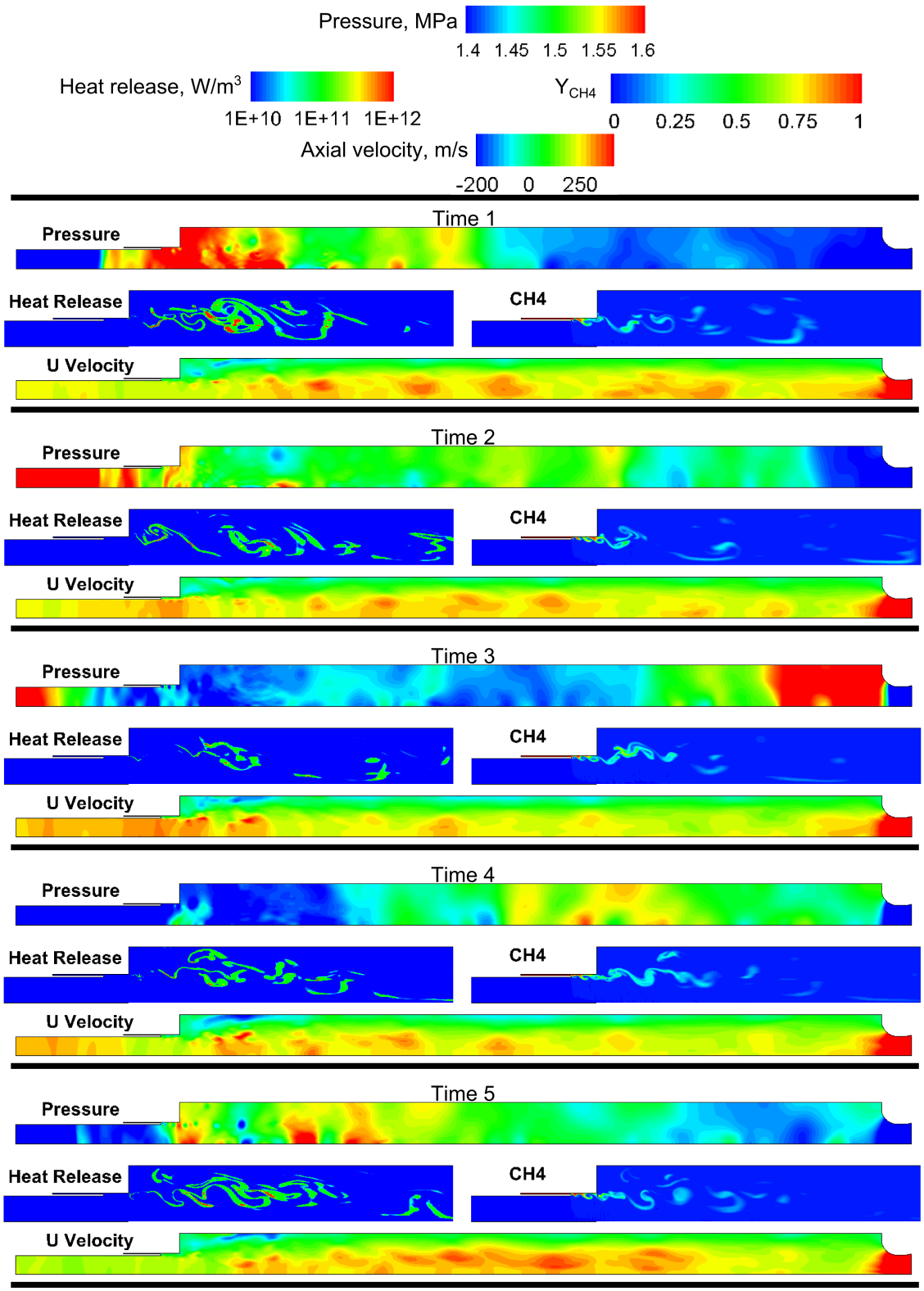

Figure 12: Limit cycle analysis for $L_{OP} = 8.89\,\text{cm}$

seen in case of the oxidizer post length of $13.97e\,\text{cm}$. Due to the increased oxidizer post length, the returning wave from the oxidizer post has yet to reach the fuel sleeve exit. At the next point of the cycle (time 4), the

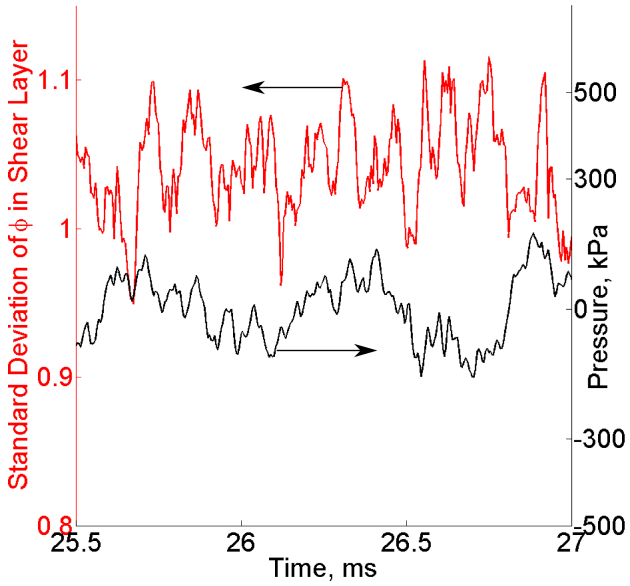

Figure 13: Shear layer unmixedness variation with pressure for the oxidizer post length 8.89 cm case.

high velocity region near the fuel injector indicates the return of pressure wave from the oxidizer post. In contrast to the 13.97e cm case, where mixing is driven by the returning oxidizer post pressure wave, shear layer roll-up and the high-velocity oxidizer stream lead to earlier mixing of the reactants and combustion products. The heat release in this case takes place before the returning wave in the oxidizer post reaches the head end of the combustor. The difference in the heat release locations between the two cases is due to this behavior. Since mixing and heat release occur earlier than the arrival of the reflected pressure wave in the combustor, the coupling of the acoustic mode and heat release mode can become weaker. This uncertain coupling can explain the borderline stability in the case of longer oxidizer post length.

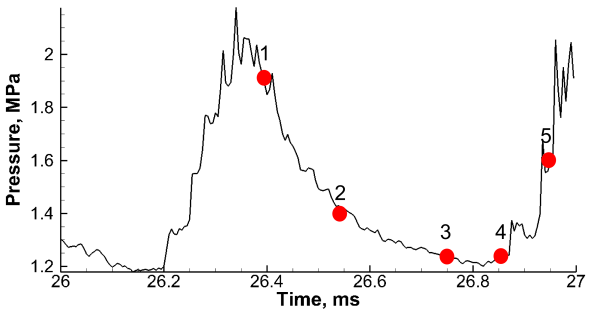

Figure 14: Pressure cycle chosen for detailed analysis of the oxidizer post length 19.05cm.

Figure 16 shows the history of equivalence ratio variation in the shear layer for the longer oxidizer post. It shows the first dip in the standard deviation due to the upstream moving pressure wave passing the fuel sleeve. A sharp second dip in the variation is observed subsequently, which suggests the role of the high velocity region formed near the fuel injector due to lower pressure at the combustor head end. Subsequent fuel accumulation and the cycle follows in the same manner as discussed before.

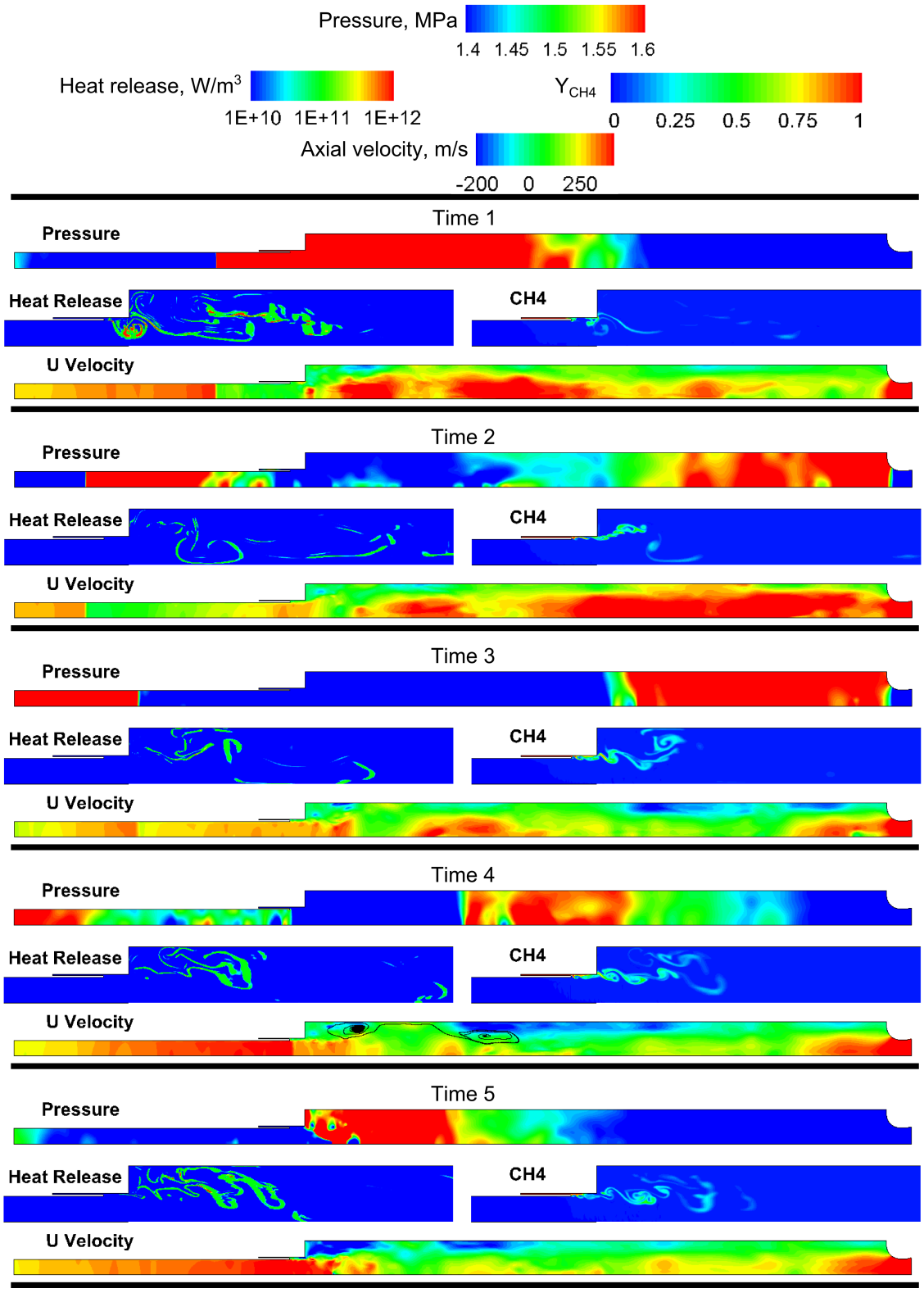

Figure 15: Limit cycle analysis for $L_{OP} = 19.05$cm

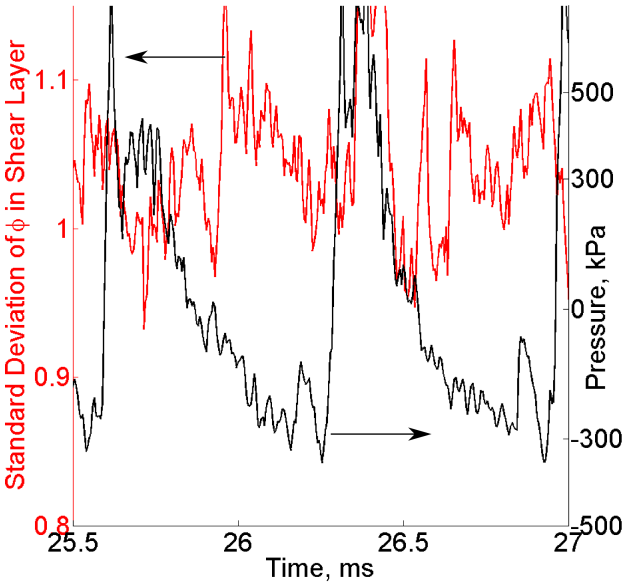

Figure 16: Shear layer history in the oxidizer post 19.05cm case, showing the early mixing due to increased oxidizer post length.

IV. Summary and Future Work

Characteristics of chemical kinetics schemes such as the ignition delay, temperature rise and heat release rate can impact the reacting flow simulations significantly. This effect is particularly noted for modeling of the combustion instability in the CVRC experiments. Although the single step kinetics scheme predicts the self-excited combustion instability, predicted frequencies exceed the observations while the amplitude of the instability is lower. The difference is more pronounced for high order harmonics where the detailed mechanism does a better job of capturing the harmonics compared to the global mechanims.

Predictions of ignition delay, temperature rise and heat release rate with the detailed mechanism - GRI-1.2 are close to that of GRI-3.0 mechanism. The use of this detailed kinetics mechanism benefits the combustion instability predictions for the CVRC experiment. The use of GRI-1.2 mechanism also enables a direct comparison with the visual measurements, which is advantageous for the transient phenomena such as combustion instability.

Simulation of the short oxidizer post length shows axially extended fuel consumption due to less traverse time for the pressure wave in the oxidizer post. Mixing in the shear layer does not deviate significantly within the cycle. For the unstable oxidizer post length of 13.97 cm, mixing within the shear layer is related to the reflected pressure wave in the oxidizer post. Formation of an upstream moving vortex acts as a precursor to the coherent heat release that occurs upon return of the pressure wave in the combustor. Similar behavior is seen for the longer oxidizer post length, but an alternative mixing mechanism is seen due to increased axial velocity near the dump plane of the combustor.

Prior simulations of CVRC have shown the marked advantage of three-dimensional simulations over two-dimensional axisymmetric models. Unrealistic oxidizer stream contraction and separation of fuel and oxidizer due to product formation are some of the disadvantages that can be eliminated in three-dimensional simulations. The computational cost of three-dimensional simulations is at least an order of magnitude higher than the axisymmetric simulations. Also of interest is the use of accurate thermal boundary condition for the combustor wall. Further, the incorporation of appropriate turbulent combustion closure may also impact the accuracy of the combustion response. The above aspects will form the basis of continued and future research investigations.

V. Acknowledgments

We gratefully acknowledge the support provided for this work by the Air Force Office of Scientific Research under the grant FA9550-14-1-0029 with Dr. Mitat Birkan as the program manager. Sincere thanks are also due to Dr. Mitsuaki Tanabe for providing the experimental data for comparison.

References

[1] Y. Yu, J. Sisco, S. Rosen, A. Madhav, and W. Anderson. Spontaneous Longitudinal Combustion Instability in a Continuously-Variable Resonance Combustor. *Journal of Propulsion and Power*, 2012.

[2] Oliver Lammel, Harald Schütz, Guido Schmitz, Rainer Lückerath, Michael Stöhr, Berthold Noll, Manfred Aigner, Matthias Hase, and Werner Krebs. Flox® combustion at high power density and high flame temperatures. *Journal of Engineering for Gas Turbines and Power*, 132(12):121503, 2010.

[3] Hukam C Mongia. Engineering aspects of complex gas turbine combustion mixers part i: High t. *AIAA Paper*, 107:4–7, 2011.

[4] R. Smith, G. Xia, W. Anderson, and C. Merkle. Computational Studies of the effects of oxidiser injector length on combustion instability. *Combustion Theory and Modeling*, 2012.

[5] M. Harvazinski, W. Anderson, , and C. Merkle. Analysis of self-excited combustion instability using two- and three- dimensional simulations. *Journal of Propulsion and Power*, 2013.

[6] M. Harvazinski, C. Huang, V. Sankaran, T. Feldman, W. Anderson, C. Merkle, and D. Talley. Instability Mechanism in a Pressure-coupled Gas-gas coaxial rocket injector. In *49th AIAA/ASME/SAE/ASEE Joint Propulsion Conference and Exhibit*, pages 1–21, San Jose, CA, July 2013. AIAA, AIAA.

[7] R. Garby, L. Selle, , and T. Poinsot. Large-Eddy Simulation of Combustion Instabilities in a Variable-length Combustor. *Comptes Rendus Mecanique*, 2013.

[8] S. Srinivasan, R. Ranjan, and S. Menon. Flame Dynamics During Combustion Instability in a High-Pressure, Shear-Coaxial Injector Combustor. *Flow Turbulence and Combustion*, 2014.

[9] Smith R., Xia G., Anderson W., and Merkle C. Computational Studies of the Effects of Oxidizer Injector Length on Combustion Instability. In *46th AIAA/ASME/SAE/ASEE Joint Propulsion Conference and Exhibit*. American Institute of Aeronautics and Astronautics, 2010.

[10] Westbrook C. and Dryer F. Simplified Reaction Mechanism for the Oxidation of Hydrocarbon Fuels in Flames. *Combustion Science and Technology*, 1981.

[11] Frenklach M., Wang H., Goldenberg M., Smith G., Golden D., Bowman C., Hanson R., Gardiner W. , and Lissianski V. GRI-Mech-1.2, An Optimized Detailed Chemical Reaction Mechanism for Methane Combustion. Technical report, Gas Research Institute, 1995.

[12] Holton M., Jackson G., Gokulakrishnan P., Klassen M., and Roby R. Autoignition delay time measurements of methane, ethane, and propane pure fuels and methane-based fuel blends. *Journal of Engineering for Gas Turbines and Power*, 132(9):091502, 2010.

[13] Wilcox C. Formulation of the $k-\omega$ Turbulence Model Revisited. *AIAA journal*, 46(11):2823–2838, 2008.

[14] Choi Y.H. and Merkle C.L. The Application of Preconditioning in Viscous Flows. *Journal of Computational Physics*, 105(2):207–223, 1993.

[15] Venkateswaran S., Lindau J.W., Kunz R.F., and Merkle C.L. Computation of Multiphase Mixture Flows with Compressibility Effects. *Journal of Computational Physics*, 180(1):54–77, 2002.

[16] Li D., Sankaran V., Lindau J.W., and Merkle C.L. A Unified Computational Formulation for Multi-Component and Multi-Phase Flows. In *43 rd AIAA Aerospace Sciences Meeting and Exhibit*, 2005.

[17] Lian C., Xia G., and Merkle C.L. Impact of Source Terms on Reliability of CFD Algorithms. *Computers and Fluids*, 39(10):1909–1922, 2010.

[18] Harvazinski M.E. *Modeling Self-Excited Combustion Instabilities Using a Combination of Two and Three-Dimensional Simulations*. PhD thesis, Purdue University, 2012.

[19] Venkata N Nori and Jerry M Seitzman. CH* Chemiluminescence Modeling for Combustion Diagnostics. *Proceedings of the Combustion Institute*, 32(1):895–903, 2009.

[20] Bryan Higgins, MQ McQuay, François Lacas, Juan-Carlos Rolon, Nasser Darabiha, and Sébastien Candel. Systematic Measurements of OH Chemiluminescence for Fuel-lean, High-pressure, Premixed, Laminar Flames. *Fuel*, 80(1):67–74, 2001.

[21] CS Panoutsos, Y Hardalupas, and AMKP Taylor. Numerical Evaluation of Equivalence Ratio Measurement Using OHâˆ— and CHâˆ— Chemiluminescence in Premixed and Non-premixed Methane-Air Flames. *Combustion and Flame*, 156(2):273–291, 2009.

[22] KT Walsh, MB Long, MA Tanoff, and MD Smooke. Experimental and computational study of ch, ch¡ sup¿*¡/sup¿, and oh¡ sup¿*¡/sup¿ in an axisymmetric laminar diffusion flame. In *Symposium (International) on Combustion*, volume 27, pages 615–623. Elsevier, 1998.